A 355-nm RAYLEIGH-MIE LIDAR USING TWO MICHELSON INTERFEROMETERS AS SPECTRAL ANALYZERS FOR MULTI-PURPOSE NEAR-FIELD MEASUREMENTS

Nicolas Cezard[(1)], Agnès Dolfi-Bouteyre[(1)], Jean-Pierre Huignard[(2)], Pierre Flamant[(3)]

[(1)] French Aeronautics and Space Research Center (ONERA), Chemin de la Hunière 91761 Palaiseau, France, E-mail: nicolas.cezard@onera.fr, agnes.dolfi-bouteyre@onera.fr
[(2)] Thales Research & Technology (TRT), Route départementale 128, 91767 Palaiseau Cedex,France, E-mail: jean-pierre.huignard@thalesgroup.com
[(3)] Dynamic Meteorology Laboratory (LMD), Ecole Polytechnique 91128 Palaiseau,France, E-Mail : flamant@lmd.polytechnique.fr

ABSTRACT

The theoretical performances of a 355 nm Rayleigh-Mie lidar for simultaneous short-range measurements of wind speed, air temperature, air density, and aerosol/molecular backscattering ratio are discussed. We propose to use two wide-angle fringe-imaging Michelson interferometers with distinct path differences as spectral analyzers. The optimization of the instrument and its theoretical best performances are calculated by evaluating the Cramer-Rao Bounds. The effect of fringe contrast on performances is also addressed, and particularly the problem of contrast loss arising from the use of a wide source such as a fiber end. By using field-compensation plates, the loss can be considerably reduced. In conclusion, the performances are simulated for typical situations at low and high altitudes.

INTRODUCTION

This work is conducted by ONERA and THALES R&T, as part of a preliminary study aiming at the design of a new multi-purpose airborne lidar to measure near-field air parameters (~ 70 m) for future active flight-control systems. Wind radial speed, air temperature, air density, and aerosol/molecular backscattering ratio are the four parameters of interest. They can be retrieved from the lidar backscattered light by spectral analysis. A system employing a fringe-imaging Fabry-Perot interferometer has been previously developed with interesting preliminary results [1]. Another approach using two-wave interferometers has also been proposed [2], which we believe could offer some practical advantages. Unfortunately, a two-wave interferometer, when used alone and without any assumption on the atmospheric properties, can only perform wind speed measurements. It is impossible to measure adequately temperature, density and backscattering ratio all at once because of the coupling between these parameters in the interferometer response (see Sec.2-3). To overcome this limitation, an additional instrument is required. In this paper we propose to use in parallel two Michelson interferometers with distinct path differences.

1. INSTRUMENT DESCRIPTION

The instrument is described in Fig.1. The laser is an injection-seeded Nd:YAG laser delivering 10 mJ/pulse at 355-nm. An obstruction mirror placed in front of a 10-cm diameter reception telescope enables selecting a near-field gate ranging between about 40-150m.

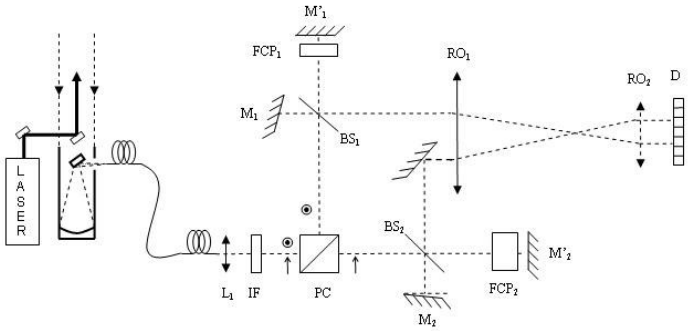

Fig. 1 : Instrument Description
L_1: Collimation lens ; IF : Interferential Filter ; PC : Polarizing Cube; $BS_{1,2}$: Beam-splitters, $FCP_{1,2}$: Field Compensation Plates; $M_{1,2}$ - $M'_{1,2}$: Michelson mirrors ($M_{1,2}$ tilted), $RO_{1,2}$: Relay Optics ; D : Detector (CCD)

The backscattered light is focused in a multimode optical fiber ensuring the opto-mechanical decoupling between the emission-reception unit and the spectral analyzer. The fiber end is located at the focus of a lens that produces a light pencil with a small but significant aperture of a few mrad. It can then be split in two parts by a polarizing cube. Each part goes through a Michelson interferometer, in which one mirror is slightly tilted to give fringes of equal thickness. The path-differences in each interferometer are several centimetres long. In such conditions, the fringe contrast obtained with a wide source is very low (see Sec.4). By inserting field-compensation plates into the longer arm of each interferometer, this contrast loss can be drastically reduced. Finally, it is possible to image the fringe pattern from the two interferometers on a single CCD camera by the mean of adequate relay optics.

2. INSTRUMENT MODELLING

2.1 Rayleigh-Mie (RM) backscattered spectrum

We assume a Gaussian lineshape for the pulsed laser. The half width at 1/e is $\gamma_L \cong 150$ MHz. This width is sufficient to consider the backscattered Mie lineshape as Gaussian. We also consider that air molecules are in the kinetic collisionless regime. We thus neglect the spontaneous Brillouin scattering and consequently, the Rayleigh lineshape is also Gaussian. The backscattered spectral density is then:

$$N(\nu) = K\rho^* \left[\frac{1}{\gamma_G(T)\sqrt{\pi}} e^{-\left(\frac{\nu-\nu_c(u_r)}{\gamma_G(T)}\right)^2} + \frac{(\alpha-1)}{\gamma_L\sqrt{\pi}} e^{-\left(\frac{\nu-\nu_c(u_r)}{\gamma_L}\right)^2} \right] \quad (1)$$

$$\gamma_G(T) = \sqrt{\sigma^2 T + \gamma_L^2} \quad \text{with} \quad \sigma = \frac{2}{\lambda_L}\sqrt{\frac{2k_B}{m}} \quad (2)$$

In Eq.1, the Rayleigh and Mie spectra are centred at the same frequency ν_c verifying $\nu_c - \nu_L = 2u_r/\lambda_L$, where u_r is the average wind speed and ν_L the laser frequency.

The term α is the usual backscattering ratio defined by $\alpha = 1 + \beta_M / \beta_R$, where β_R and β_M are the Rayleigh and Mie backscattering coefficients respectively.

Air density fluctuations are accounted by a normalized air density parameter noted $\rho^* = \rho / \rho_0$, where ρ_0 is a reference density.

The backscattered energy is scaled by a factor K that can be obtained during the instrumental calibration. It is the total number of photons backscattered in clear air and at reference density (α=1, $\rho = \rho_0$).

In Eq.2, T is the temperature, k_b the Boltzmann constant and m the molecular mass for air.

2.2 Detected signal

In this instrument the CCD-detector play the role of a multi-channel analyzer, where each channel is defined as a pixel row aligned parallel to the fringes. Following a similar approach as in [2], the number of photoelectrons observed on the k-th channel for a single Michelson interferometer can be written:

$$S_k(u_r, \rho^*, T, \alpha) = \frac{K\eta}{4P}\rho^*\alpha \times \ldots$$
$$\left[1 + V\left(\frac{1}{\alpha} e^{-\left(\frac{\pi\sigma\Delta_0}{c}\right)^2 T} + \left(1 - \frac{1}{\alpha}\right) \right) \cos\left(\frac{4\pi\Delta_0}{c\lambda_L} u_r + \phi(k) \right) \right] \quad (3)$$

$$\text{with} \quad V = V_{field}\,\mathrm{sinc}(1/P)\, e^{-\left(\frac{\pi\gamma_L\Delta_0}{c}\right)^2} \quad (4)$$

In Eq.3, η is the quantum efficiency of the detector. The definition of K can be modified so that it includes additional transmission factors. However, we neglect the atmospheric absorption because the lidar range is short. The term Δ_0 is the path difference of the interferometer and P the number of pixel per fringe period. The function $\phi(k)$ is the phase of the fringe-pattern at zero radial speed. The contrast factor V, defined in Eq.4, arises from various phenomena reducing the fringe pattern contrast (see Sec.4).

Equations 3-4 can be used to model the signals delivered by the two interferometers, changing only the value of the path-difference. These equations rely on simplifying assumptions (one fringe period is illuminated; the illuminating spot is a square). We use this model for clarity in this paper, but the method presented in the next section is straightforwardly applicable to more realistic situations.

3. INSTRUMENT OPTIMIZATION

3.1 Cramer-Rao Bounds (CRBs)

We gather in a single parameter vector $\vec{\theta} = (u_r, \rho^*, T, \alpha)$ the four parameters of interest. The generalization of the Cramer-Rao inequality in the case of a multi-parameter estimation states that, for an unbiased estimator, the Cramer-Rao Bounds (minimal quadratic error of any estimator) are defined as the diagonal terms of the inverse Fisher information matrix. Assuming independent channels (no cross-talk) and shot-noise limited detection, this matrix is:

$$F_{ij} = \sum_{k=1}^{P} \frac{1}{S_k} \frac{dS_k}{d\theta_i} \frac{dS_k}{d\theta_j} \qquad (5)$$

This is for a single interferometer. The matrix of the whole instrument is the sum of the matrices associated with each interferometer. From Eq.3 and Eq.5 it is found that the matrix of the instrument takes the form:

$$F = \begin{bmatrix} F_{11} & 0 & 0 & 0 \\ 0 & F_{22} & 0 & F_{24} \\ 0 & 0 & F_{33} & F_{34} \\ 0 & F_{24} & F_{34} & F_{44} \end{bmatrix} \qquad (6)$$

Equation 6 makes formal the fact that speed measurements are independent from the other measurements. The CRB on wind speed is simply $\varepsilon_{u_r}^{CRB} = 1/F_{11}$. As said in introduction, a single interferometer is sufficient for speed measurements (see also [2]). On the other hand, Eq.6 shows that there is some correlation between variables (ρ^*, α) and (T, α). For a single interferometer, this coupling is such that neither of them can be retrieved: there are three unknowns acting on only two measurable quantities: the energy and fringe contrast. But by adding a second interferometer with a distinct path-difference, supplementary information is provided that enables the decoupling of these three parameters.

To optimize the instrument, we can look for the optimal values of the path-differences that yield the minimal CRBs for the parameters we are most interested in. Here we choose to optimize the instrument for wind speed measurements in clear air conditions (α=1), with temperature measurement as secondary goal. Density and backscattering ratio are considered as spin-off products of the measurement.

3.2 Wind speed optimization

Here we can consider a single Michelson interferometer because it is sufficient for speed measurements. Using Eq.3 in Eq.5, the CRB for speed measurements in clear air is found to be:

$$\varepsilon_{u_r} = \frac{c\lambda_L}{4\pi\Delta_0} \sqrt{\frac{4}{K\eta\rho^*}} \left(1 - \sqrt{1 - V^2 \, e^{-2\left(\frac{\pi\sigma\Delta_{01}}{c}\right)^2 T}} \right)^{-\frac{1}{2}} \qquad (7)$$

The CRB is proportional to $K^{-1/2}$, an expected result in shot-noise limited measurements. Equation 7 is plotted as a function of Δ_{01} and V on Fig.2. From Eq.7 we see, however, that an optimal value can be found only for a specified working temperature of the atmosphere: we choose T=273K. We also use a calibration constant $K=10^6$, a realistic value for a 10 mJ pulse with the range gate previously mentioned, and a CCD quantum efficiency η=0.5.

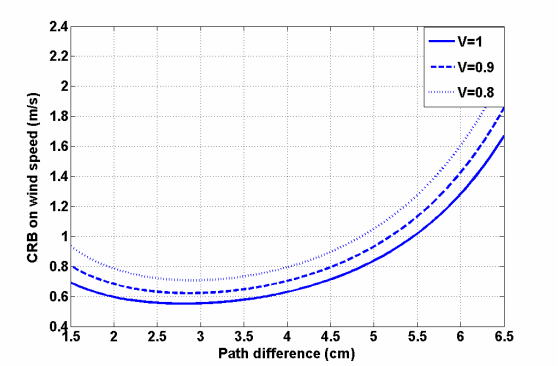

Fig.2 Optimization of the first Michelson for wind speed

The optimal path-difference for speed measurements is Δ_{01}=2.8 cm, a result previously found in [2] following a different approach. Figure 2 illustrates the need to obtain the best possible contrast factor V. Though the accuracy for V=0.8 is reduced only by a factor about 1.4, it is important to realize that one should double the laser energy in order to compensate this loss.

3.3 Temperature optimization

We use now two interferometers. The first one is set with Δ_{01}=2.8 cm, and to determine the path difference Δ_{02} of the second interferometer, we use Fig.3 where the temperature CRB is plotted as a function of Δ_{02}. The setup conditions are still α=1 and T=273°K. Unit contrast factors are taken for each interferometer.

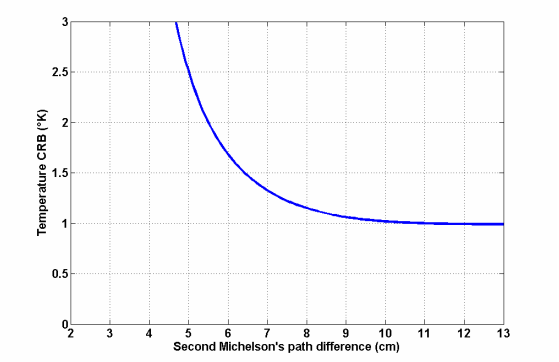

Fig.3 Optimization of the second Michelson for temperature

Figure 3 shows that there is only little improvement by choosing Δ_{02} longer than 10 cm. It also shows, when compared with Fig.2, that at constant energy the accuracy on temperature measurement is less than for wind speed. Finally, a good compromise for the path-difference settings is (Δ_{01}=2.8 cm, Δ_{02}=10 cm).

4. FRINGE CONTRAST

Equation 4 highlights the contrast losses arising from the finite spatial resolution of the detector (sinc-term) and from the spectral width of the laser source (exp-term). These two factors are not critical however: the former is about 99% as soon as P>12 and the latter is 99.8% for the short Michelson interferometer and 97.5% for the long one (referred MI_1 and MI_2 next).
We shall focus on the term named V_{field} in Eq.4, which comes from the combined use of a wide source with important path differences. Here the source is the exit of a fiber of 200 µm core-diameter at the focus of a lens of focal length 24 mm: the angular half-aperture is then ρ_{max}=4.1 mrad. The factor of contrast in the localization plane is:

$$V_{field} = \left| \mathrm{sinc}\left(\frac{\Delta_0 \rho_{\max}^2}{2\lambda} \right) \right| \qquad (8)$$

Using Eq.8 with Δ_{01}=2.8 cm and Δ_{02}=10 cm leads to the dashed and dotted curves in Fig.4. The fringe contrasts at ρ_{max}=4.1 mrad are very low.

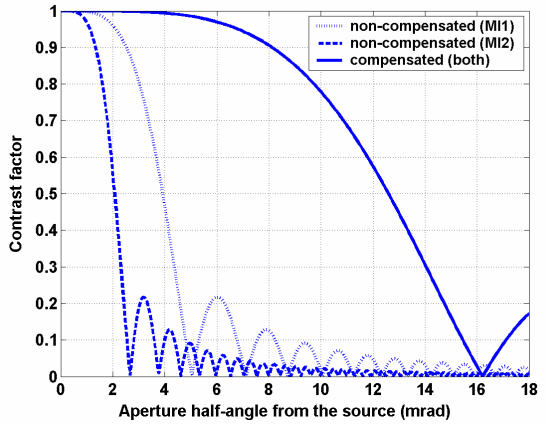

Fig.4 Effect of field-compensation on contrast

By inserting field-compensation plates in the long arm of each interferometer, one can overcome the problem. This technique has been first described in [3]. However, the use of a thick plate beamsplitter introduces an asymmetry in the angular dependence of the path-differences between different pairs of rays inside the interferometer. Thus only a partial compensation can be designed which is limited by the thickness of the beamsplitter. But at low angles this partial compensation is nevertheless very efficient (solid curve in Fig.4). Using this technique, the contrast losses should be negligible even with 4-5 mrad aperture angles.

5. SIMULATED PERFORMANCES

We give here some numerical values of the CRBs calculated from the simplified model of Eq.3. We hold K=10^6 and η=0.5. Contrast factors V_1 and V_2 are 0.9.
For the evaluation of performance at ground level, we calculate the CRBs for ρ*=1, T=288K, and α=2. For an evaluation at high altitude, we use ρ*=0.25 (11000m), T=223K, α=1. The results are in table 1.

Table.1 Numerical simulation of performances

	ε_{ur} (m/s)	$\varepsilon_{\rho*}$ (%)	ε_T (°K)	ε_α
Ground	0.1	0.2	1.7	0.004
11000 m	1.1	0.08	2.4	0.003

The most demanding parameter is the temperature, but averaging a few pulses should make possible to reach accuracies below the degree.

CONCLUSION

A new instrument has been presented for the simultaneous measurements of several air parameters. A method to optimize the instrument performances has been presented. The method can be applied to more realistic situations including Brillouin contribution and round fringe patterns. A breadboard is currently in development at ONERA.

REFERENCES

[1]. P.Tchoryk, C.Watkins, S.Lindemann, P.Hays, C.Nardell, « Molecular Optical Air Data System (MOADS) », *Laser Radar Technology and Applications VI, SPIE Proc.* Vol. 4377 (2001)

[2]. Bruneau « Fringe-imaging Mach-Zehnder interferometer as a spectral analyzer for molecular Doppler wind Lidar », *Appl.Opt.* Vol.41, n°3, p.503 (2002)

[3]. Hilliard, Shepherd, "Wide-angle Michelson Interferometer for Measuring Doppler Line Widths", *JOSA*, Vol.56, n°3, p.362 (1966)